First-principles investigation of CuO decomposition and its transformation into Cu 2 O

Hicham Jabraoui, Mehdi Djafari Rouhani, Carole Rossi, Alain Estève

First principles investigation of CuO decomposition and its transformation into Cu_2O

Hicham Jabraoui, Mehdi Djafari Rouhani, Carole Rossi, Alain Esteve

LAAS-CNRS, University of Toulouse, 31077 Toulouse, France

Abstract

This paper reports on the mechanisms of CuO decomposition and its associated phase transformation into Cu_2O, as a fundamental step of thermite materials reaction, where CuO serves as the oxidizer. Frenkel pair defects in perfect bulk CuO show extremely high formation energy (>4 eV) indicating that its decomposition initiates at defects/interfaces/surfaces, the latter being sensitive to surface orientation. In contrast to a variety of CuO surfaces ((111), (110), $(10\bar{1})$) exhibiting three-fold coordinated oxygen atoms, results show that oxygen vacancy formation requires higher disordered surfaces, such as the CuO(001), on which the vacancy formation activation energy is reduced to 1.31 eV. This leads to the exothermic formation of a chemisorbed O-O peroxy-bridge complex at the surface (-1.25 eV adsorption), that thermodynamically moderates the backreaction (vacancy annihilation). Further desorption of molecular oxygen necessitates an activation of 1.53 eV, compatible with CuO decomposition observed experimentally at 600 K (~second process duration). As a driving mechanism of oxygen release upon decomposition, migrations of the vacancy close to the surface and towards the bulk are determined for a number of crystalline directions and surface orientations and

shows considerable anisotropy, with two preferential directions: [110] and [001] with 1.35 and 1.77 eV activation, lowered to 1.08 and 1.03 eV activation when approaching the (111) and (001) surfaces, respectively. Finally, the CuO to Cu_2O phase transformation follows a two-step process: a first structural modification from monoclinic to orthorhombic takes place when CuO has lost 12.5% of its oxygen atoms, followed by a barrierless transition to the cubic phase when 44-48% of the oxygen atoms have been removed, i.e., very close to stoichiometric Cu_2O.

I. INTRODUCTION

CuO is among the most promising multi-functional materials for different science and technological applications including gas sensing [1–4], biomedical [5], catalysis [6] and nanoenergetics [7–13]. Over the past two past decades, nanoenergetic materials have received a growing attention due to their rapid energy release rates, their use as additives in conventional energetic materials [14], and their possible use in microsystems based applications [15–18]. In most formulations, aluminum is used as a fuel in association with a CuO oxidizer showing high energy density and low cost. Indeed, the metastability of the Cu-O bonds positioned close to strong metallic acceptors, such as aluminum, titanium or zirconium species, makes it a very effective oxidizer [19]. Several works reported that nanoscale aluminum and copper oxide initiate at temperature varying from 670 to 850 K and deflagrate with combustion velocities varying between 100 and 1000 $m.s^{-1}$ depending on several factors among which are the gaseous environment, confinement and size of reactants [20–24]. The general question that still remains of interest is how do these mixtures ignite and react depending on the environment and heating conditions. Some works recently suggest that the reactivity of thermite mixtures is highly correlated with the thermal decomposition and oxygen release of oxidizer rather than the overall thermochemistry [25,26]. Indeed, two possible initiation mechanisms have been proposed to explain the different initiation and reaction regimes observed in Al/CuO thermites. The first

mechanism states that condensed phase reactions may occur by the diffusion of oxygen through solid and molten phases of Al and CuO across their shared interfaces [27–29], prior to full CuO decomposition. Considering this mechanism, dominant in fully-dense composites, the initiation temperature is reduced (670 K) compared to powdered thermites (~850 K) [30,31]. Alternatively, a gas phase reaction pathway may occur by the reduction of the metal oxide first (i.e., $CuO \rightarrow Cu_2O$) which releases gaseous oxygen [25], thus allowing the metallic fuel to burn (i.e., $Al \rightarrow Al_2O_3$) in an oxidizing environment (oxygen released by the CuO decomposition). The correlation between oxygen release and nanothermite reaction have been suggested by Umbrajkar et al. [9] and Abdallah et al. [32]. Both tentatively concluded that the appearance of the first exothermic Differential Scanning Calorimetry (DSC) peak at ~ 570 K should correspond to an indirect signature of the decomposition of the oxide into Cu_2O and gaseous oxygen. Later, a direct experimental evidence of the correlation between the oxygen release from the CuO and the initiation of nanothermites was given by Zhou et al. [25] using a T-Jump time of flight mass spectrometer under high heating rate (10^5 $K.s^{-1}$). Altogether, these experimental works highlight that the temperature at which O_2 is released from the CuO plays a critical role in the ignition mechanism of Al/CuO nanothermites. Unfortunately, the current knowledge about the exact mechanisms of CuO decomposition (pathways and their kinetics) and the impact of heating rate and environment is totally unclear, limiting the rigorous interpretation of these experimental observations to further optimize the Al/CuO nanothermite systems. As a first step towards the understanding of CuO decomposition in various environments, such as the chemical nature of an oxidizing atmosphere or the fuel material being in contact (Al, Zr, B …), this density functional theory (DFT) study aims at identifying and quantifying the energetics and pathways by which CuO decomposition is operated, and how CuO will transform into Cu_2O as O_2 is released under vacuum conditions.

This paper addresses two questions. One is dedicated to the identification of mechanistic pathways responsible for the release of oxygen from CuO, the other being dedicated to the understanding of CuO to Cu_2O phase transformation. We propose that the decomposition mechanism is driven by the presence of oxygen vacancies (V_O): preexisting or being generated at specific defective surfaces, such as on the CuO(001) surface. In this frame, O_2 can be released after overcoming a double activation energy of successively 1.31 eV and 1.53 eV. The kinetics of oxygen released from the CuO network is detailed and can proceed through migration via vacancy sites, associated with an activation energy of 1.35 eV in bulk, that reduces to 1 eV when reaching the surface. We theoretically show that this scenario is site and surface specific. Finally, CuO phase transformation into Cu_2O is calculated to be a two-step process: volume shape accommodation to orthorhombic cell at the early stage of oxygen loss and finally, barrierless transition to the cubic phase at the very end of the oxygen release (48% of oxygen loss).

II. COMPUTATIONAL DETAILS

All calculations were performed using the DFT periodic Vienna *ab initio* Simulation Package (VASP) [33]. Since conventional DFT functionals cannot provide a good description of the strong correlation effect between partially filled 3d Cu states in CuO [34], DFT +U calculations were performed using the Perdew-Burke-Ernzerhof (PBE) density functional and the Projected Augmented Wave method (PAW) while the plane wave cutoff energy was set at 500 eV [35]. Spin-polarized calculations were performed as the CuO bulk exhibits an antiferromagnetic ground state. Atomic positions were fully optimized up to all forces were less than 0.02 eV/Å per atom. The Kohn–Sham (KS) equations were solved self-consistently until the energy difference between cycles reach a value smaller than 10^{-6} eV [36–38]. The Brillouin-zone

sampling was restricted to the Γ-point. To take into account van der Waals interactions in our calculations, we used the semi empirical scheme D2 developed by Grimme [39]. So far, this method shows promising results for describing adsorption and desorption phenomena [37,40,41]. The climbing image nudged elastic band (CI-NEB) method [42] was used with six intermediate images between the initial and the final states to model the diffusion path and calculate the activation energy. In this paper, we will call formation energy the net total energy difference between two (meta)stable configurations of a given system, that will be noted as ΔE. The activation energy is defined by the energy difference between a system in a (meta)stable configuration and a given saddle point at its proximity, i.e., the minimum quantity of energy which the reacting species must possess in order to undergo a specific reaction (noted as E_a). While the formation energy defines the thermodynamic balance between two configurations, the activation energy is at the basis of the kinetics of the evolving system.

A CuO supercell was built, characterized by a monoclinic symmetry with space group C2/c1 and lattice parameters being a = 4.684 Å, b = 3.423 Å, c = 5.129 Å, α = γ = 90° and β = 99.45° [43,44]. The bulk CuO supercell was obtained by replicating the conventional unit-cell in all three directions by 2×4×2 factors (see **Figure 1a),** leading to 64 Cu atoms and 64 O atoms content. Several surfaces were built, namely CuO(111), (110), $(10\bar{1})$ and (001), to investigate how the surface orientation affects the activation energy of the vacancies generation/migration, and finally CuO reduction as an outcome of O_2 release. The CuO(111) surface was considered herein because it is quasi systematically detected on X Ray Diffraction (XRD) patterns obtained on sputtered-CuO thin films used in Al/CuO nanoenergetics such as those shown in references [45]. It has to be noted that sputtered-CuO is columnar, suggesting that a variety of more or less perpendicular planes should coexist on the lateral surfaces of the columns, or at grain boundaries. Therefore, we also consider the (001) surface (see **Figure 1b** and **Figure 1c**)

as being a less stable orientation, known experimentally to enhance catalytic properties, exhibiting undercoordinated surface oxygen atoms, as well as on more stable CuO(110) and $(10\bar{1})$ surfaces, also often observed in XRD patterns [46]. Note that no dipole corrections were used for polar surfaces, for which thicker vacuum space was considered to avoid artifacts. Consistently, this choice was also motivated by a combination of electron diffraction and High Resolution Transmission Electron Microscopy (HRTEM) analysis showing that while CuO nanoparticles mainly show the compact and stable (111) orientation of the monoclinic structure, CuO nanobelts exhibit CuO(001) planes [36]. Noteworthy, the CuO(001) undergoes surface reconstruction, allowing part of the surface oxygen atoms to satisfy their dangling bonds thanks to the upward motion of copper atoms from the subsurface to the surface (see Supplemental Material **S1.1** for full description [47]).

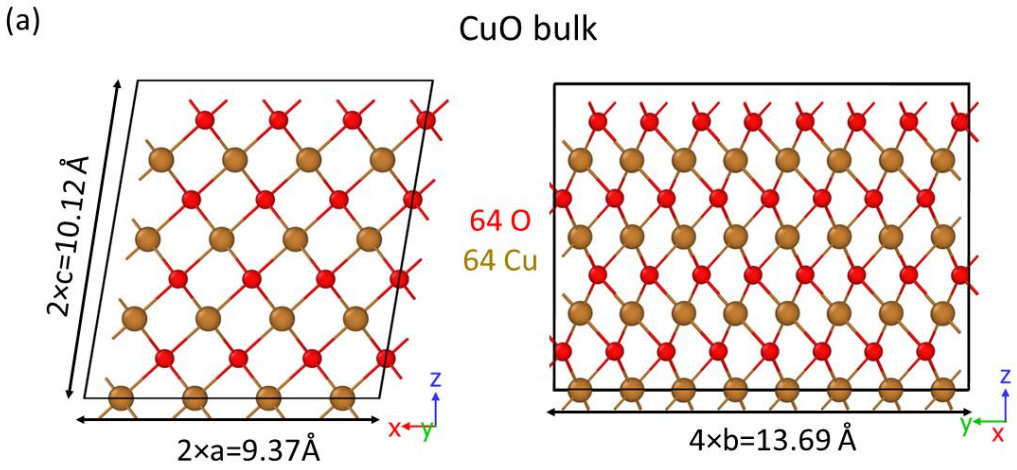

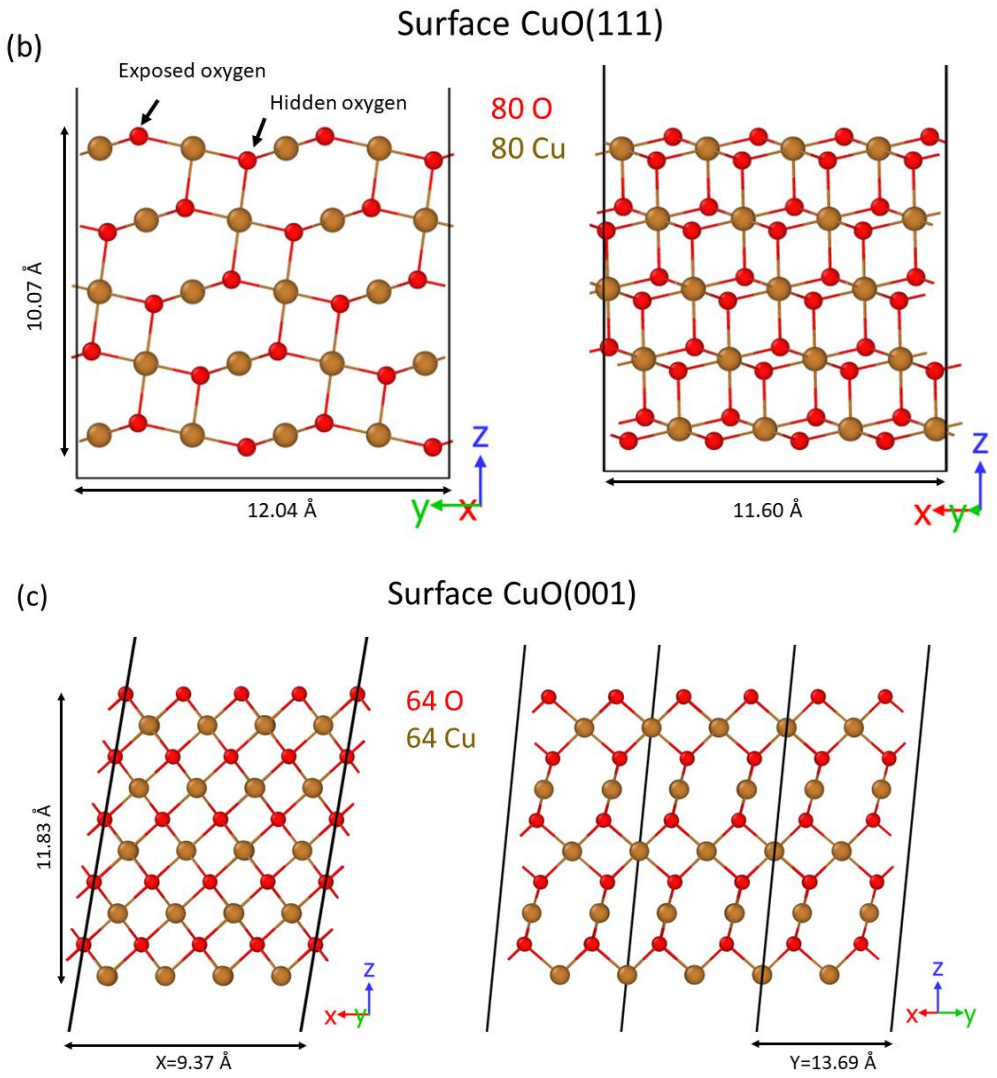

Figure 1. Slab side views of main supercell dimensions and structures: (a) bulk CuO, (b) CuO(111) surface and (c) unreconstructed CuO(001) surface, side views. The red and light brown balls represent oxygen and copper atoms, respectively. This color choice is used throughout the document. All other surface orientations are given in Supplemental Material **S1.2** [47].

III. RESULTS AND DISCUSSION

CuO decomposition into Cu_2O is a challenging process to compute, as it is characterized by a mass loss (loss of half of its oxygen content) accompanied with a monoclinic CuO to cubic Cu_2O transformation. In fact, comparing the molecular volumes using DFT lattice parameters (see **Table 2**), we find 20.52 $Å^3$ and 20.12 $Å^3$ for CuO and Cu_2O, respectively, so the lattice volume remains roughly unchanged after CuO decomposition. This indicates that Cu_2O could be considered, to some extent, approximately equivalent to CuO with half of oxygen atoms reallocated to interstitial sites. Moreover, disregarding these interstitial oxygen atoms (further noted as I_O), CuO and Cu_2O feature a topological equivalence, with only slight change in the oxygen positions relative to Cu ones, and assuming shape accommodation between cubic and monoclinic phases of Cu_2O and CuO, respectively: in both crystals, aside lattice relaxation, (i) the copper atoms occupy the same positions, and, (ii) (001) planes of oxygen atoms alternate with (001) Cu planes (see Supplemental Material **Figure S2** for a schematic view of atom locations and planes [48]). Along this line, transforming CuO into Cu_2O is equivalent to grab half of the oxygen atoms from their CuO lattice sites, the remaining lattice oxygen only undergoing minor changes. This pleads for a gradual reduction where oxygen is released from the CuO matrix while Cu atoms follow only the lattice relaxation along the monoclinic to cubic phase transformation (CuO → Cu_2O). In this context, oxygen release can basically proceed through oxygen migration as interstitial, subsequently to Frenkel defect formation (i.e., a process in which lattice oxygen atoms migrate to interstitial sites, leaving oxygen vacancy sites (noted as V_O). As vacancies are being created, new and energetically more favorable pathways, via V_O sites, might be considered for oxygen migration. In the next sections, the energetics and pathways of these elementary mechanisms are calculated in order to depict a possible scenario of the CuO decomposition in vacuum. CuO bulk and surfaces (CuO(111), (110), $(10\bar{1})$ and (001)) are considered for mechanisms evaluation. In a last section, based on minimum energy paths, the occurrence of CuO → Cu_2O phase transformation is discussed.

A. CuO decomposition nucleation, energetics and pathways

Decomposition initiation through oxygen vacancy formation –

Table 1 gives the formation energy (ΔE) and activation energies (E_a) via CI-NEB calculations, considering a collection of mechanisms in relation with the potential decomposition scenario discussed in the previous section, i.e., I_O/V_O generation (Frenkel defect), migration, and surface oxygen release. Considering CuO bulk, 4.80 eV is required to generate the Frenkel defect in which a lattice oxygen migrates to the nearest oxygen interstitial site. We conclude that this process is not relevant regarding the experimental CuO decomposition temperature found at ~600 K in vacuum [20,24,41]. Indeed, at an elevated temperature, as 1600 K, the process would take a few minutes to be operated. This indicates that the release of oxygen atoms cannot be initiated from perfect bulk CuO, but rather at defective or surface/interface sites. Noteworthy, the activation energy corresponding to the migration of an interstitial oxygen atom in perfect CuO is found to be also substantially large, equals to 2.84 eV along the preferential [110] direction, which is accompanied with a non-zero energy budget for the formation energy (0.12 eV), due to differences in the local environment of the initial and final positions of the migrating oxygen, because monoclinic CuO exhibits two distinct Cu-O distances.

Table 1: Formation and activation energies (*via* CI-NEB calculations) of a selection of mechanisms, on various CuO configurations, bulk and surfaces.

CuO system	**Mechanism**	**Formation energy ΔE (eV)**	**Activation energy E_a (eV)**
Bulk	Frenkel defect formation	4.80	4.80
	Migration (O interstitial)	0.12	2.84
	Surface vacancy/peroxy bridge	2.06	3.30

Surface (111)	Monovacancy formation	2.41*	6.88
	Divacancy formation*/O_2 release**	5.38*	3.32**
Surface (001)	Surface vacancy/peroxy-bridge	-1.25	1.31
	Monovacancy formation	-0.07*	4.40
	Divacancy formation*/O_2 release**	0.28*	1.53**

*Vacancy and divacancy type of defects are referenced to the perfect (or reconstructed) surface, and creation of ½ or 1 O_2 molecule, respectively; ** activation referred to as the energy required to desorb O_2 from its adsorbed position.

Considering the CuO(111) surface, the lowest energetic path to create a V_O is to form a peroxy-bridge resulting from the displacement of a surface oxygen atom towards its nearest oxygen neighbor along the surface oxygen row as shown in **Figure 2a**. In this configuration, the O-O axis is perpendicular to the oxygen rows, so that oxygen atoms can bridge surface copper atoms in adjacent copper rows. The activation energy to perform this displacement is 3.30 eV, with a loss in energy of 2.06 eV. On this surface, the direct V_O creation, without peroxy-bridge formation, still requires a prohibitive formation energy of 2.41 eV, characterized by an even more prohibitive activation energy, superior to 6 eV. From the peroxy-bridge configuration, releasing O_2 still requires another prohibitive 3.32 eV activation energy. In conclusion, oxygen species cannot be released by CuO(111).

Exploring now the CuO(001) surface, the V_O creation leads to the formation of a peroxy-bridge configuration different from that of the CuO(111), as it is now oriented along the surface oxygen rows. Interestingly, the activation energy is considerably lowered, down to 1.31 eV, and the

reaction is associated with an energy gain of -1.25 eV. This underlines the metastability of the CuO(001) for which defects may act as stabilizing agents of the overall surface. This behavior could be similar to the well documented polar ZnO(0001) surface [51,52] exhibiting triangular pit and/or missing oxygen rows type of defects to compensate for the surface extra-charge of the non-defective surface. The identification of these defects was made possible by using extended experimental (TEM, thermal desorption spectroscopy)/theoretical (DFT) studies, which could be advantageously produced for characterizing the chemistry of CuO(001) type of surfaces. Considering now the ability of CuO(001) to release one oxygen molecule from the peroxy-bridge configuration, we calculate an activation energy of 1.53 eV, which greatly improves the release rate compared to the CuO(111) surface (3.32 eV). Note that releasing atomic oxygen, while being thermodynamically favorable, is completely unfeasible from a kinetic viewpoint (4.40 eV activation energy). **Figure 2b** details the structures along the chemical path. While reconstruction allows maximizing the coordination of surface atoms, making it possible for each surface oxygen atom to have three bonds with copper atoms underneath, reconstruction induces displacement of copper atoms in the immediate sublayer that disrupts some of their bonds. This results in the shortening of surface Cu-O bonds (2 peaks in the pair correlation function at 1.87 and 1.93 Å compared with the unique 1.96 Å value for the CuO(111), (see Supplemental Material file **Figure S1.2** [47]). The stabilization of the surface concomitantly with the creation of defects is one probable explanation for its capability to generate vacancy sites. To consolidate this hypothesis, we also considered several other stable surfaces with natural 3-fold coordination. They all showed activation energies above 3 eV (see Supplemental Material **S3.1** and **3.2** for the CuO(110), CuO(010) and CuO(101) surfaces [49]). In addition, it is important to emphasize that the creation of the V_O onto CuO(001) quasi coincides with the direct formation of an O_2 molecule. The structure shown in **Figure 2b** gives the final structure, along the path to vacancy creation. The O-O orientation is

parallel to the surface oxygen rows of atoms, while the peroxy-bridge axis is oriented perpendicular to the rows in the case of the CuO(111) surface. This results in a O-O bond length of 1.29 Å for CuO(001), very close to the diatomic molecule O_2 bond length in the gas phase (1.21 Å), versus 1.48 Å for the O-O bond length on CuO(111) (see **Figure 1b**). Note that some of the O-Cu bonds of the CuO(001) peroxy-bridge configuration are stretched from 1.87 to 3.40 Å, consistently showing that these bonds are almost broken. However, there is still a 1.53 eV activation energy to overcome for transforming the CuO(001) peroxy-bridge into a O_2 molecule distant from the surface. Importantly, the aggregated divacancy on the (111) and (001) surfaces is less stable than 2 spread vacancies, by 0.56 eV and 0.42 eV, respectively. This is also the case in bulk, for which the cost in aggregating two vacancies is 0.20 eV. These values are consistent with the formation of Cu_2O since massive reduction of CuO through vacancy aggregation would lead to the direct formation of pure copper aggregates.

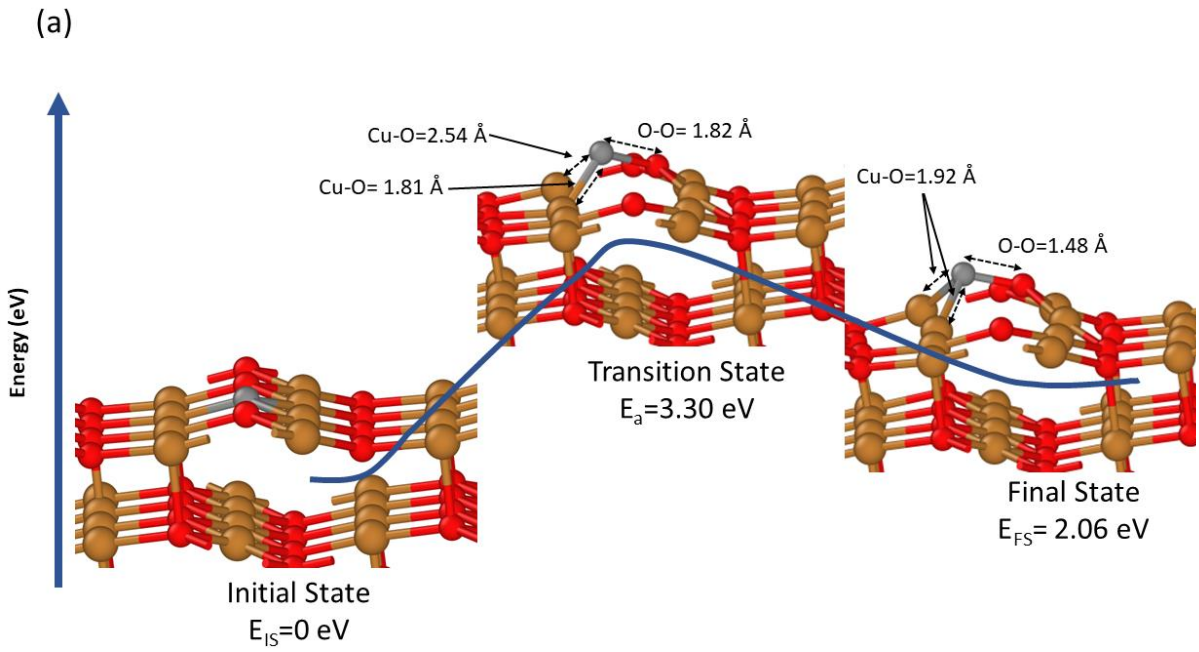

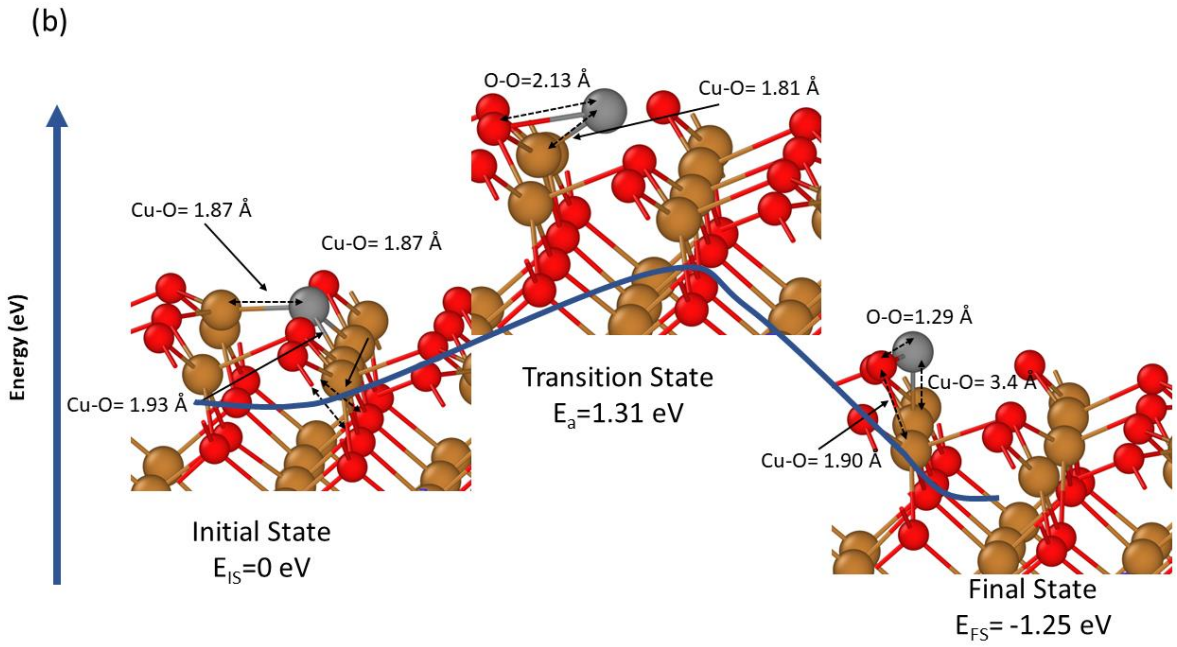

Figure 2. Creation of surface oxygen vacancy through oxygen migration towards nearest neighbors oxygen on (a) CuO(111) and (b) CuO(001) surfaces. Pathways as determined by CI-NEB. The red and light brown balls represent oxygen and copper atoms, respectively, while the gray ball represents the migrating oxygen atom.

Io migration kinetics. Now, we focus on the I_O migration within bulk CuO, CuO(111) and CuO(001) surfaces and subsurfaces (**Table 1** and **Figure 3**). From **Table 1**, the migration of oxygen in perfect bulk CuO via interstitial sites requires 2.84 eV. An alternative is to achieve oxygen migration across CuO via hopping steps through Vo sites. Considering the a priori presence of a single Vo in the CuO bulk supercell, **Figure 3** presents an atomistic view and all calculated energy paths as determined by CI-NEB, required for the migration of one O atom through the Vo site, as a function of crystal directions. We observe a highly anisotropic mapping of migration paths: [110] and [001] directions are the two preferential pathways exhibiting the lowest activation energies, 1.35 eV and 1.77 eV, respectively (see **Figure 3a)**. All other directions ([101], [111], [100]) show prohibitive energy paths, with activation above 2.5 eV. These possible oxygen diffusion pathways are consistent with previous published data in a joint

experimental/theoretical study [53], with slight deviations possibly emanating from different choices in DFT parameters.

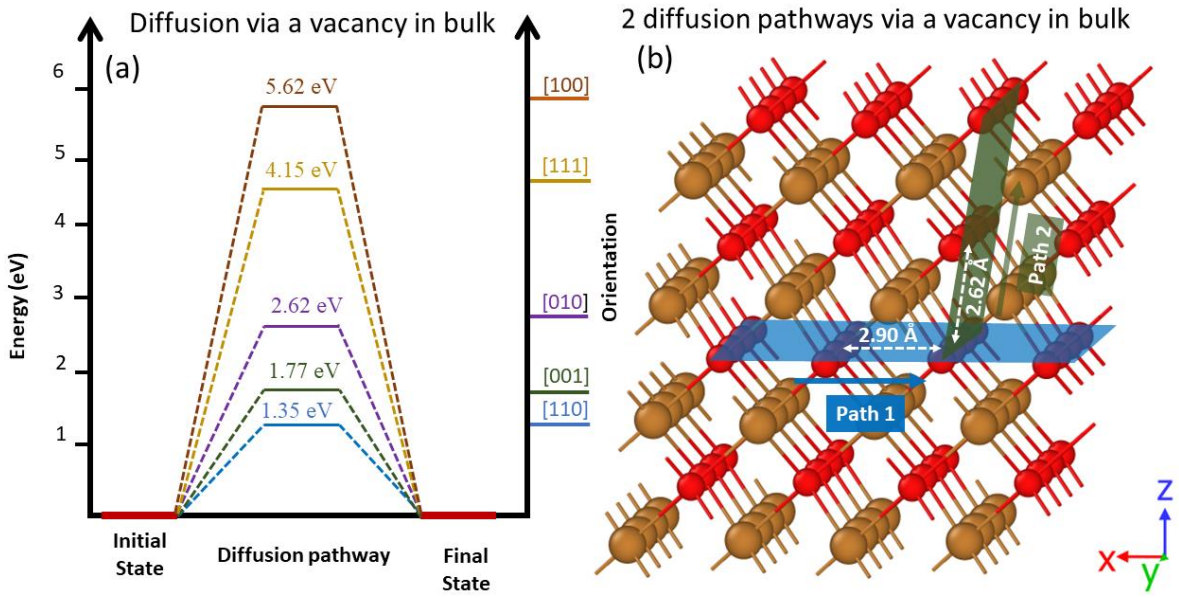

Figure 3. (a) Energetics (activation energies calculated using the CI-NEB method) and (b) bulk CuO atomistic view of oxygen migration path through oxygen vacancy sites. In (b), the two possible oxygen migration pathways are colored: in blue for the pathway following the [110] direction and, in green for the pathway following the [001] direction. The red and light brown balls represent oxygen and copper atoms, respectively.

Approaching the surface, the migration energy may change, as for the migration direction, which is addressed next (see **Figure 4**). On the CuO(111) subsurface, the migration activation energy along the [110] is lowered from 1.35 to 1.08 eV, which is associated with a slight gain in energy (by 0.15 eV). But as seen previously, oxygen cannot be released from this surface at a reasonable temperature, limiting the interest of this surface for CuO decomposition.

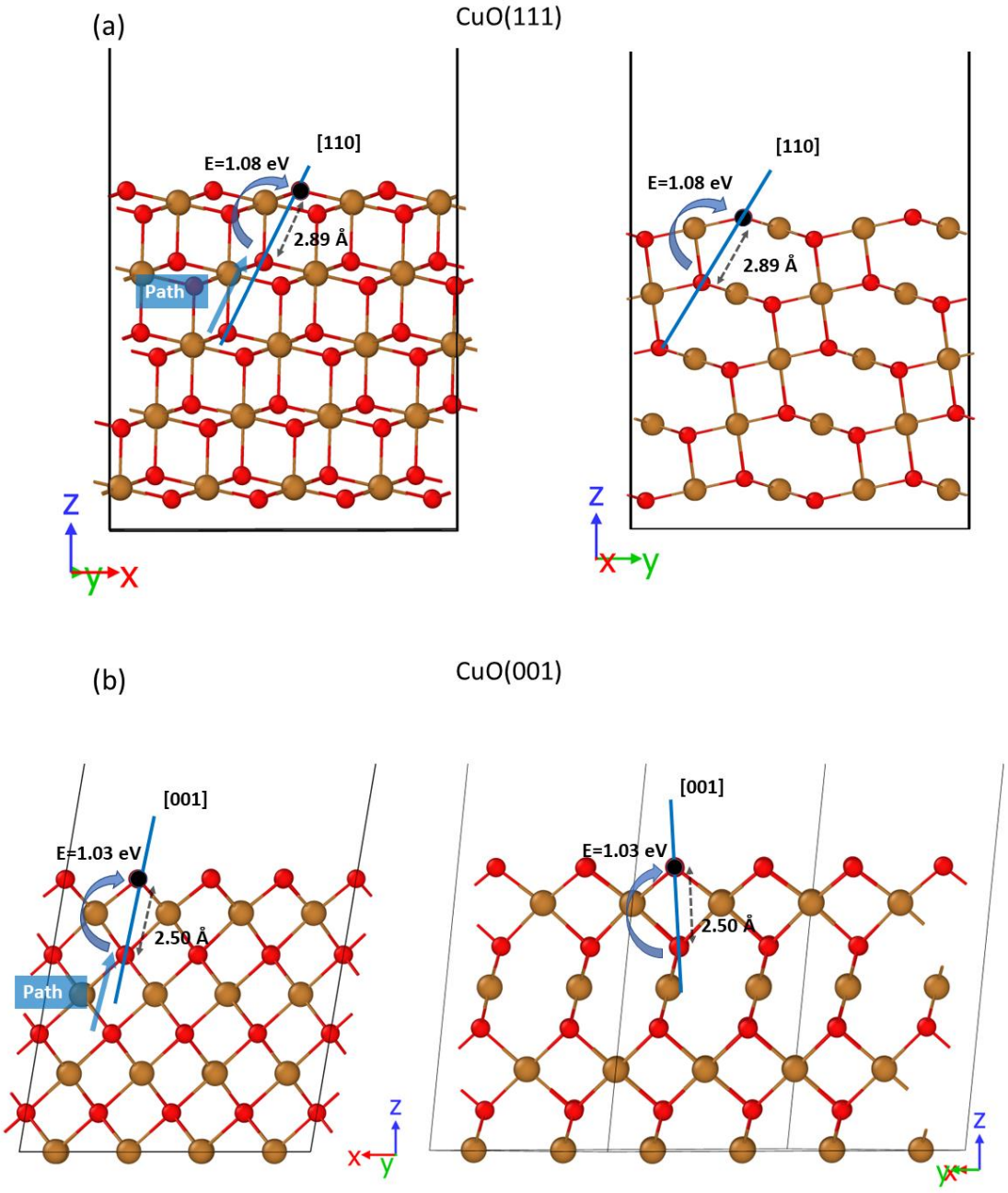

Figure 4. Side views of oxygen migration pathways from bulk to (a) CuO (111) and (b) CuO(001) surfaces via vacancy and their activation energies as calculated by CI-NEB. The red and light brown balls represent oxygen and copper atoms, respectively. Note that the CuO(001) views are kept unreconstructed for more clarity.

Approaching the (001) surface, as for the (111) case, the migration activation energy is lowered in the direction perpendicular to the surface, being 1.03 eV, which is to be compared with the 1.77 eV obtained in bulk CuO. In contrast to CuO(111), this last step of oxygen migration to the top surface is endothermic by 0.86 eV, which may be another confirmation of the behavior of the (001) surface to get stabilized by removing part of its surface oxygen atoms. Overall, these calculations suggest that V_O are needed to assist the transport of oxygen towards the surface and its subsequent release from CuO. Generally, non-defective and stable CuO surfaces (with natural three-fold coordination of surface oxygen atoms) are not prone to initiate the decomposition because the activation energy is too prohibitive to displace oxygen atoms from their network positions at temperatures lower than 1000 K, similarly to what is obtained in perfect bulk CuO. In this context, we calculate that Vo can be generated only on specific surface orientations, such as the (001) plane (≈1.5 eV needed for desorbing O_2 from the surface and creating two vacancies). The findings on CuO(001), for which the non-reconstructed surface exhibits only two fold coordination of surface oxygen atoms, could be considered as a model surface. Indeed, surface defects play a dual role, in enhancing the surface chemical reactivity and potentially stabilizing the surface energy. In this frame, not only the migration of oxygen towards the surface is enhanced (~1 eV activation energy), but also promotes the desorption of O_2 molecules at the cost of 1.53 eV energy. Making now the link to experimental data, the columnar growth morphology is usually observed in physically grown nanolayers, mainly exhibiting the (111) orientation at the columns top terminations (seen in XRD patterns). Other planes, more or less perpendicular to (111) can therefore be present along grain boundaries, in which the defective nature should also promote undercoordinated forms of oxygen configurations, including CuO(001) surfaces. This scenario is consistent with experimental studies showing that CuO nanoplatelets exhibiting (001) surface orientation more readily release oxygen from the surface and are more chemically active than nanoparticles having

CuO(111) orientation [50]. Also, in a more recent experimental study on Al/CuO nanothermite, the authors observed Cu_2O after annealing the CuO at 600 K [24]. Considering the migration activations of (i) Io through the bulk (1.35 eV), (ii) through the CuO(001) subsurface (1.03 eV) and (iii) for generating the surface peroxy-bridge complex (1.31 eV), the kinetic limiting step for oxygen release from CuO remains the desorption of the peroxy-complex to form free O_2:. 1.53 eV energy cost. From the latter value, the O_2 release is estimated in the order of the second at 600 K, which agrees with in situ infrared experiments presented in Ref [54].

B. CuO to Cu_2O phase transformation

Having established the effective release of oxygen atoms from bulk CuO, we now consider several concentrations of oxygen vacancies and calculate how these affect the overall structure, e.g., the volume and shape of the CuO cell. From perfect monoclinic bulk CuO presented in the simulation cell of 2×4×2 conventional unit-cell, containing 64 oxygen atoms, we suggest four structures with increasing vacancy (V_O) concentrations: 8, 16, 24, and 32 V_O structures are fully optimized by letting the atomic positions, shape cell, and volume cell relax freely upon DFT+U calculations. The last structure corresponds to the stoichiometric Cu_2O, but still within a non-cubic cell. Obviously, the choice of oxygen vacancy locations is an issue. Since the aggregation of vacancies is not energetically favorable, as discussed earlier, we choose distant vacancies (as far as possible) while respecting a regular distribution, in order to keep a homogeneous lattice structure. Despite the fact that a large number of structures satisfy the intermediate V_O concentrations, their energetics are such that the specifically chosen structures allow unambiguous response for the identification of the phase transformation.

Table 2. The lattice parameters resulting from different chemical compositions during the CuO transformation into Cu_2O, after full minimization of atomic positions as well as volume and

cell shape. Total energy is defined as the as calculated DFT total energy of a given configuration. Relative energy means the energy difference between a specified configuration and a reference configuration (see notes * and **).

Vacancy number (system)	Total energy (eV)	Relative energy*,** (eV)	a	b	c	α	β	γ
0, (CuO)	-573.85	0*	4.68	3.42	5.13	90	99.54	90
8, (Cu_8O_7)	-515.63	-58.23*	4.42	3.61	5.15	90.02	91.96	89.97
16, (Cu_4O_3, Paramelaconite)	-454.81	-119.05*	4.46	3.51	5.08	90.04	91.03	89.96
24, (Cu_8O_5)	-412.46	-161.4*	4.24	3.7	5.01	89.94	89.96	89.93
32, (Cu_2O)	-372.19	-201.66*	4.51	3.78	4.54	89.99	90.15	90.00
Cubic Cu_2O	-372.58	-0.39**	a=b=c=4.29			α = β = γ =90.00		

* The reference energy corresponds to the total energy of the CuO configuration

** Perfect cubic Cu_2O energy relative to Cu_2O value undergoing phase transformation (i.e., non equal a, b and c).

We observe that angles of conventional monoclinic unit cell shift to the 90° value readily at the first step (8 vacancies) upon our suggested pathway, underlying the fact that the monoclinic to orthorhombic transition is taking place at an early stage, as CuO deoxidizes. Increasing more the vacancy concentration allows convergence of the lattice parameters to Cu_2O values: a and c axis decreasing from 4.68 and 5.13 to 4.51 and 4.54 Å, respectively, when reaching the Cu_2O stoichiometry. The b axis, being 3.42 Å for CuO, naturally stretches to 3.78 Å, which is slightly below the Cu_2O cubic value (4.29 Å). In this way, we obtain an orthorhombic structure that is very close to the cubic structure of Cu_2O. Comparing the tetragonal and cubic Cu_2O structures in **Table 2**, we find that the cubic structure is actually the most stable, by 0.39 eV, leaving the

orthorhombic Cu_2O as a metastable state corresponding to a secondary minimum. Importantly, the 0.39 eV value distinguishing both structures is surprisingly very low, so that the two structures are very close in energy. We perform now a reverse process, by adding extra oxygen atoms, one by one, diminishing the total Vo from 32 to 24 units, within the cubic Cu_2O matrix, minimizing the energy, authorizing volume breathing, but constraining the cell to its cubic form. **Figure 5a** shows the calculated values in black triangles, to be compared with the blue curve (non-cubic CuO). For more clarity, **Figure 5b** proposes a differential plot of the cubic versus orthorhombic structure. Results indicate that a crossing over of the 2 energy paths is taking place when considering the range 28-30 Vo (44-48% of oxygen loss from the initial CuO structure). Below this amount of Vo defects, the cubic structure quickly becomes unlikely from an energetic point of view, with a lowering of 1.5 eV when the oxygen loss represents 40% of the oxygen population in CuO. This energy difference then largely increases when reducing the number of oxygen vacancies. This indicates that the transition occurs at around 44-48% of oxygen loss. The energy difference curve is very flat in this range of vacancy concentration, and the transition only exhibits small energy changes. In order to check for the kinetic aspects of these transitions, we did select potential structure candidates (performing single point energy calculations) for making the transition from Cu_2O to CuO having 32 oxygen vacancies (maximum deviation in the **Figure 5b** plateau), for which the total energy difference is 0.39 eV. No activation was obtained. Despite the arbitrary nature of the selected structures, results give reasonable indication that the phase transformation should be quasi-barrierless.

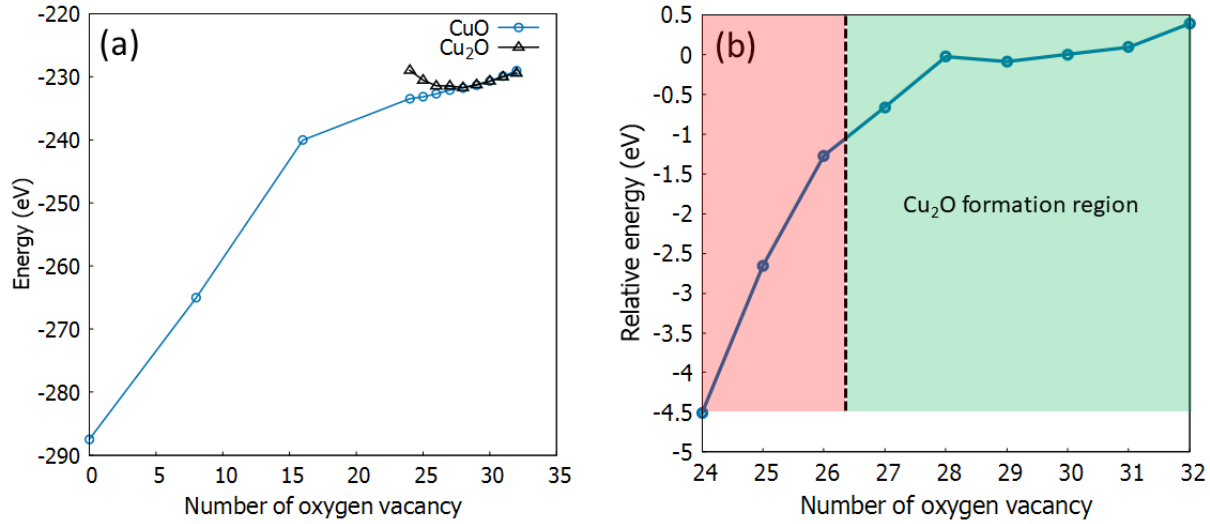

Figure 5. (a) DFT energy of copper oxide upon chemical and cell modification (volume and shape) from CuO to Cu_2O (blue scatter line) and from Cu_2O to CuO, with chemical composition transformation using a fixed cubic unit-cell, allowing relaxation of the volume and atomic positions (black scatter line). Note that the energy is here referenced to the formation of O_2. Note also that CuO into Cu_2O transformation in blue is performed varying the unit cell shape and volume while Cu_2O into CuO transformation uses a fixed cubic unit cell. (b) at each chemical composition, the plot gives the relative energy between the Cu_xO_ys [blue versus black curves of (a)].

The process proposed here allows a smooth and barrierless transition from the monoclinic CuO to cubic Cu_2O. The kinetic limiting factor in this process is the rearrangement of vacancies from their natural stochastic positions to the ordered structure proposed here. This vacancy redistribution is governed by the vacancy migration activation energy, calculated in section A "*Io migration kinetics*". This migration is also at the origin of CuO-Cu_2O phase transformation and therefore does not really inhibit the process. Another possibility, not investigated in this paper, is the precipitation of Cu_2O particles in CuO, to lead to diphasic structure. This

precipitation mechanism necessitates the knowledge of CuO/Cu_2O interface energies with various orientations. Furthermore, we also should know the kinetics of precipitate agglomeration from nano to micro and macro scales. This agglomeration can only be achieved via collective motion of atoms which probably requires long times or high temperatures.

IV. CONCLUSION

This paper reports on the identification (energetics and chemical pathways) of the atomic scale mechanisms responsible for CuO decomposition, leading to the formation of Cu_2O. We demonstrate that neither perfect bulk CuO nor perfect and stable CuO surfaces ((111), (110), (10-1) can initiate the decomposition (O_2 release energies >3 eV), which requires also the migration of oxygen atoms across the bulk to reach the surface. Rather, we calculate that decomposition can proceed through vacancy formation and migration, facilitating oxygen transport towards the surface with subsequent release in the form of O_2. Out of pre-existing oxygen vacancies, they are generated at defective surfaces, such as the CuO(001), used here as a model surface, for which the release of molecular oxygen requires overcoming a double barrier of 1.31 eV and 1.53 eV activation, respectively to create a peroxy-bridge on the surface and to desorb this complex as an O_2 molecule. Once created, we determined that the vacancies can spread into the bulk following preferential [001] (1.03 eV activation) and [110] (1.35 eV activation) routes across CuO(001) surface and bulk CuO, respectively. We expect this vacancy nucleation scenario to be effective at the grain boundaries of CuO columnar thin films (physical vapor deposition) found in conventional thermite multilayers, either because the (001) plane orientation might be present, but also because of the defective nature of the grain boundaries. Finally, we show that CuO to Cu_2O phase transformation follows a two-step process, with tetragonal to orthorhombic transition occurring after that a few percent of the oxygen atoms

have been removed from the CuO matrix, while the transformation into the cubic Cu_2O phase is performed barrierless when removing 43% of oxygen atoms.

Acknowledgement

The authors gratefully acknowledge support from the European Research Council (H2020 Excellent Science) Researcher Award (grant 832889-PyroSafe). This work was performed using computing resources from CALMIP.

References

[1] S. Keerthana and K. Rathnakannan, *Hierarchical ZnO/CuO Nanostructures for Room Temperature Detection of Carbon Dioxide*, Journal of Alloys and Compounds **897**, 162988 (2022).
[2] M. Censabella, V. Iacono, A. Scandurra, K. Moulaee, G. Neri, F. Ruffino, and S. Mirabella, *Low Temperature Detection of Nitric Oxide by CuO Nanoparticles Synthesized by Pulsed Laser Ablation*, Sensors and Actuators B: Chemical **358**, 131489 (2022).
[3] R. Bosigo, L. M. Lepodise, G. Chimowa, and C. Muiva, *Enhanced Ethanol Sensing Response of Nanostructured Ce-Doped CuO Thin Films*, Materials Chemistry and Physics **280**, 125841 (2022).
[4] T. Bhowmick, A. Ghosh, S. Nag, and S. B. Majumder, *Sensitive and Selective CO2 Gas Sensor Based on CuO/ZnO Bilayer Thin-Film Architecture*, Journal of Alloys and Compounds **903**, 163871 (2022).
[5] M. Li, X. Yin, H. Shan, C. Meng, S. Chen, and Y. Yan, *The Facile Preparation of PBA-GO-CuO-Modified Electrochemical Biosensor Used for the Measurement of α-Amylase Inhibitors' Activity*, Molecules **27**, 8 (2022).
[6] C. Cao, L. Yu, Y. Xie, W. Wei, and H. Jin, *Hydrogen Production by Supercritical Water Gasification of Lignin over CuO–ZnO Catalyst Synthesized with Different Methods*, International Journal of Hydrogen Energy **47**, 8716 (2022).
[7] Y. Zhang, H. Sui, Y. Li, and J. Z. Wen, *Energetic Characteristics of the Al/CuO Core-Shell Composite Micro-Particles Fabricated as Spherical Colloids*, Thermochimica Acta **689**, 178656 (2020).
[8] A. Ermoline, D. Stamatis, and E. L. Dreizin, *Low-Temperature Exothermic Reactions in Fully Dense Al–CuO Nanocomposite Powders*, Thermochimica Acta **527**, 52 (2012).
[9] S. M. Umbrajkar, M. Schoenitz, and E. L. Dreizin, *Exothermic Reactions in Al–CuO Nanocomposites*, Thermochimica Acta **451**, 34 (2006).
[10] K. J. Blobaum, A. J. Wagner, J. M. Plitzko, D. Van Heerden, D. H. Fairbrother, and T. P. Weihs, *Investigating the Reaction Path and Growth Kinetics in CuOx/Al Multilayer Foils*, Journal of Applied Physics **94**, 2923 (2003).
[11] J. Zapata, A. Nicollet, B. Julien, G. Lahiner, A. Esteve, and C. Rossi, *Self-Propagating Combustion of Sputter-Deposited Al/CuO Nanolaminates*, Combustion and Flame **205**, 389 (2019).

[12] G. Lahiner, A. Nicollet, J. Zapata, L. Marín, N. Richard, M. D. Rouhani, C. Rossi, and A. Estève, *A Diffusion–Reaction Scheme for Modeling Ignition and Self-Propagating Reactions in Al/CuO Multilayered Thin Films*, Journal of Applied Physics **122**, 155105 (2017).
[13] H. Wang, B. Julien, D. J. Kline, Z. Alibay, M. C. Rehwoldt, C. Rossi, and M. R. Zachariah, *Probing the Reaction Zone of Nanolaminates at ∼μs Time and ∼μm Spatial Resolution*, J. Phys. Chem. C **124**, 13679 (2020).
[14] D. L. Reid, A. E. Russo, R. V. Carro, M. A. Stephens, A. R. LePage, T. C. Spalding, E. L. Petersen, and S. Seal, *Nanoscale Additives Tailor Energetic Materials*, Nano Lett. **7**, 2157 (2007).
[15] L. J. Currano and W. A. Churaman, *Energetic Nanoporous Silicon Devices*, Journal of Microelectromechanical Systems **18**, 799 (2009).
[16] L. Glavier, A. Nicollet, F. Jouot, B. Martin, J. Barberon, L. Renaud, and C. Rossi, *Nanothermite/RDX-Based Miniature Device for Impact Ignition of High Explosives*, Propellants, Explosives, Pyrotechnics **42**, 308 (2017).
[17] J.-L. Pouchairet and C. Rossi, *PyroMEMS as Future Technological Building Blocks for Advanced Microenergetic Systems*, Micromachines **12**, 2 (2021).
[18] L. Salvagnac, S. Assie-Souleille, and C. Rossi, *Layered Al/CuO Thin Films for Tunable Ignition and Actuations*, Nanomaterials **10**, 10 (2020).
[19] J. B. DeLisio, F. Yi, D. A. LaVan, and M. R. Zachariah, *High Heating Rate Reaction Dynamics of Al/CuO Nanolaminates by Nanocalorimetry-Coupled Time-of-Flight Mass Spectrometry*, J. Phys. Chem. C **121**, 2771 (2017).
[20] T. Wu, B. Julien, H. Wang, S. Pelloquin, A. Esteve, M. R. Zachariah, and C. Rossi, *Engineered Porosity-Induced Burn Rate Enhancement in Dense Al/CuO Nanothermites*, ACS Appl. Energy Mater. **5**, 3189 (2022).
[21] H. Jabraoui, A. Esteve, M. Schoenitz, E. L. Dreizin, and C. Rossi, *Atomic Scale Insights into the First Reaction Stages Prior to Al/CuO Nanothermite Ignition: Influence of Porosity*, ACS Appl. Mater. Interfaces **14**, 29451 (2022).
[22] M. Petrantoni, C. Rossi, L. Salvagnac, V. Conédéra, A. Estève, C. Tenailleau, P. Alphonse, and Y. J. Chabal, *Multilayered Al/CuO Thermite Formation by Reactive Magnetron Sputtering: Nano versus Micro*, Journal of Applied Physics **108**, 084323 (2010).
[23] E. J. Mily, A. Oni, J. M. LeBeau, Y. Liu, H. J. Brown-Shaklee, J. F. Ihlefeld, and J.-P. Maria, *The Role of Terminal Oxide Structure and Properties in Nanothermite Reactions*, Thin Solid Films **562**, 405 (2014).
[24] M. Mursalat, C. Huang, B. Julien, M. Schoenitz, A. Esteve, C. Rossi, and E. L. Dreizin, *Low-Temperature Exothermic Reactions in Al/CuO Nanothermites Producing Copper Nanodots and Accelerating Combustion*, ACS Appl. Nano Mater. **4**, 3811 (2021).
[25] L. Zhou, N. Piekiel, S. Chowdhury, and M. R. Zachariah, *Time-Resolved Mass Spectrometry of the Exothermic Reaction between Nanoaluminum and Metal Oxides: The Role of Oxygen Release*, J. Phys. Chem. C **114**, 14269 (2010).
[26] G. Jian, S. Chowdhury, K. Sullivan, and M. R. Zachariah, *Nanothermite Reactions: Is Gas Phase Oxygen Generation from the Oxygen Carrier an Essential Prerequisite to Ignition?*, Combustion and Flame **160**, 432 (2013).
[27] G. Xiong, C. Yang, and W. Zhu, *Interface Reaction Processes and Reactive Properties of Al/CuO Nanothermite: An Ab Initio Molecular Dynamics Simulation*, Applied Surface Science **459**, 835 (2018).
[28] C. Lanthony, J.-M. Ducéré, A. Estève, C. Rossi, and M. Djafari-Rouhani, *Formation of Al/CuO Bilayer Films: Basic Mechanisms through Density Functional Theory Calculations*, Thin Solid Films **520**, 4768 (2012).
[29] G. C. Egan, T. LaGrange, and M. R. Zachariah, *Time-Resolved Nanosecond Imaging of Nanoscale Condensed Phase Reaction*, J. Phys. Chem. C **119**, 2792 (2015).
[30] L. Glavier, G. Taton, J.-M. Ducéré, V. Baijot, S. Pinon, T. Calais, A. Estève, M. Djafari Rouhani, and C. Rossi, *Nanoenergetics as Pressure Generator for Nontoxic Impact Primers: Comparison of*

Al/Bi2O3, Al/CuO, Al/MoO3 Nanothermites and Al/PTFE, Combustion and Flame **162**, 1813 (2015).
[31] E. Yao, N. Zhao, Z. Qin, H. Ma, H. Li, S. Xu, T. An, J. Yi, and F. Zhao, *Thermal Decomposition Behavior and Thermal Safety of Nitrocellulose with Different Shape CuO and Al/CuO Nanothermites*, Nanomaterials **10**, 4 (2020).
[32] I. Abdallah, J. Zapata, G. Lahiner, B. Warot-Fonrose, J. Cure, Y. Chabal, A. Esteve, and C. Rossi, *Structure and Chemical Characterization at the Atomic Level of Reactions in Al/CuO Multilayers*, ACS Appl. Energy Mater. **1**, 1762 (2018).
[33] G. Sun, J. Kürti, P. Rajczy, M. Kertesz, J. Hafner, and G. Kresse, *Performance of the Vienna Ab Initio Simulation Package (VASP) in Chemical Applications*, Journal of Molecular Structure: THEOCHEM **624**, 37 (2003).
[34] L. Wang, T. Maxisch, and G. Ceder, *Oxidation Energies of Transition Metal Oxides within the $\mathrm{GGA}+\mathrm{U}$ Framework*, Phys. Rev. B **73**, 195107 (2006).
[35] C. Ricca, L. Grad, M. Hengsberger, J. Osterwalder, and U. Aschauer, *Importance of Surface Oxygen Vacancies for Ultrafast Hot Carrier Relaxation and Transport in ${\mathrm{Cu}}_{2}$O*, Phys. Rev. Research **3**, 043219 (2021).
[36] I. Khalil, H. Jabraoui, S. Lebègue, W. J. Kim, L.-J. Aguilera, K. Thomas, F. Maugé, and M. Badawi, *Biofuel Purification: Coupling Experimental and Theoretical Investigations for Efficient Separation of Phenol from Aromatics by Zeolites*, Chemical Engineering Journal **402**, 126264 (2020).
[37] H. Jabraoui, I. Khalil, S. Lebègue, and M. Badawi, *Ab Initio Screening of Cation-Exchanged Zeolites for Biofuel Purification*, Mol. Syst. Des. Eng. **4**, 882 (2019).
[38] P. Losch, H. R. Joshi, O. Vozniuk, A. Grünert, C. Ochoa-Hernández, H. Jabraoui, M. Badawi, and W. Schmidt, *Proton Mobility, Intrinsic Acid Strength, and Acid Site Location in Zeolites Revealed by Varying Temperature Infrared Spectroscopy and Density Functional Theory Studies*, J. Am. Chem. Soc. **140**, 17790 (2018).
[39] S. Grimme, *Semiempirical GGA-type density functional constructed with a long-range dispersion correction*, Journal of Computational Chemistry **27**, 1787 (2006).
[40] H. Jabraoui, T. Charpentier, S. Gin, J.-M. Delaye, and R. Pollet, *Behaviors of Sodium and Calcium Ions at the Borosilicate Glass–Water Interface: Gaining New Insights through an Ab Initio Molecular Dynamics Study*, The Journal of Chemical Physics **156**, 134501 (2022).
[41] H. Jabraoui, T. Charpentier, S. Gin, J.-M. Delaye, and R. Pollet, *Atomic Insights into the Events Governing the Borosilicate Glass–Water Interface*, J. Phys. Chem. C **125**, 7919 (2021).
[42] G. Henkelman, B. P. Uberuaga, and H. Jónsson, *A Climbing Image Nudged Elastic Band Method for Finding Saddle Points and Minimum Energy Paths*, J. Chem. Phys. **113**, 9901 (2000).
[43] D. P. Volanti, M. O. Orlandi, J. Andrés, and E. Longo, *Efficient Microwave-Assisted Hydrothermal Synthesis of CuO Sea Urchin-like Architectures via a Mesoscale Self-Assembly*, CrystEngComm **12**, 1696 (2010).
[44] A. Catana, J.-P. Locquet, S. M. Paik, and I. K. Schuller, *Local Epitaxial Growth of CuO Films on MgO*, Phys. Rev. B **46**, 15477 (1992).
[45] C. Rossi, *Engineering of Al/CuO Reactive Multilayer Thin Films for Tunable Initiation and Actuation*, Propellants, Explosives, Pyrotechnics **44**, 94 (2019).
[46] V. Singh, B. Julien, L. Salvagnac, S. Pelloquin, T. Hungria, C. Josse, M. Belhaj, and C. Rossi, *Influence of Process Parameters on Energetic Properties of Sputter-Deposited Al/CuO Reactive Multilayers*, Nanotechnology (n.d.).
[47] See Supplemental Material at [] for further description of CuO model surfaces.

[48] See Supplemental Material at [] for description of the CuO (001) plane topology.

[49] See Supplemental Material at [] for description of CuO(10-1), (110) and (010) surfaces and associated surface oxygen vacancy formation.

[50] K. Zhou, R. Wang, B. Xu, and Y. Li, *Synthesis, Characterization and Catalytic Properties of CuO Nanocrystals with Various Shapes*, Nanotechnology **17**, 3939 (2006).
[51] A. Önsten, D. Stoltz, P. Palmgren, S. Yu, M. Göthelid, and U. O. Karlsson, *Water Adsorption on ZnO(0001): Transition from Triangular Surface Structures to a Disordered Hydroxyl Terminated Phase*, J. Phys. Chem. C **114**, 11157 (2010).
[52] M. Iachella, J. Cure, M. Djafari Rouhani, Y. Chabal, C. Rossi, and A. Estève, *Water Dissociation and Further Hydroxylation of Perfect and Defective Polar ZnO Model Surfaces*, J. Phys. Chem. C **122**, 21861 (2018).
[53] L. Li et al., *Room-Temperature Oxygen Vacancy Migration Induced Reversible Phase Transformation during the Anelastic Deformation in CuO*, Nat Commun **12**, 1 (2021).
[54] J. Kwon, J. M. Ducéré, P. Alphonse, M. Bahrami, M. Petrantoni, J.-F. Veyan, C. Tenailleau, A. Estève, C. Rossi, and Y. J. Chabal, *Interfacial Chemistry in Al/CuO Reactive Nanomaterial and Its Role in Exothermic Reaction*, ACS Appl. Mater. Interfaces **5**, 605 (2013).